ACS APPLIED MATERIALS & INTERFACES

Research Article

www.acsami.org

Growth and Characterization of Al_2O_3 Atomic Layer Deposition Films on sp^2-Graphitic Carbon Substrates Using NO_2/Trimethylaluminum Pretreatment

Matthias J. Young,[†] Charles B. Musgrave,[†,‡] and Steven M. George*[,‡,§]

[†]Department of Chemical and Biological Engineering, University of Colorado, Boulder, Colorado 80309, United States

[‡]Department of Chemistry and Biochemistry, University of Colorado, Boulder, Colorado 80309, United States

[§]Department of Mechanical Engineering, University of Colorado, Boulder, Colorado 80309, United States

ABSTRACT: The growth of Al_2O_3 films by atomic layer deposition (ALD) on model sp^2-graphitic carbon substrates was evaluated following a nitrogen dioxide (NO_2) and trimethylaluminum (TMA) pretreatment to deposit an Al_2O_3 adhesion layer. Al_2O_3 ALD using TMA and water (H_2O) as the reactants was used to grow Al_2O_3 films on exfoliated highly ordered pyrolitic graphite (HOPG) at 150 °C with and without the pretreatment procedure consisting of five NO_2/TMA cycles. The Al_2O_3 films on HOPG substrates were evaluated using spectroscopic ellipsometry and electrochemical analysis to determine film thickness and quality. These experiments revealed that five NO_2/TMA cycles at 150 °C deposited an Al_2O_3 adhesion layer with a thickness of 5.7 ± 3.6 Å on the HOPG substrate. A larger number of NO_2/TMA cycles at 150 °C deposited thicker Al_2O_3 films until reaching a limiting thickness of ∼80 Å. Electrochemical impedance spectroscopy (EIS) measurements revealed that five cycles of NO_2/TMA pretreatment enabled the growth of high quality insulating Al_2O_3 films with high charge-transfer resistance after only 20 TMA/H_2O Al_2O_3 ALD cycles. In contrast, with no NO_2/TMA pretreatment, EIS measurements indicated that 100 TMA/H_2O Al_2O_3 ALD cycles were necessary to produce an insulating Al_2O_3 film with high charge-transfer resistance. Al_2O_3 films grown after the NO_2/TMA pretreatment at 150 °C were also demonstrated to have better resistance to dissolution in an aqueous environment.

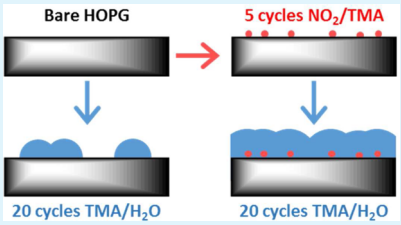

KEYWORDS: *thin film, nucleation, surface chemistry, electrochemistry, charge-transfer resistance, porosity, dissolution*

I. INTRODUCTION

The growth of ultrathin and continuous metal oxide films by atomic layer deposition (ALD) on sp^2 carbon surfaces, including graphene and carbon nanotubes, is important for a variety of applications.[1] One application is metal oxide ALD to deposit dielectric layers for graphene or carbon nanotube transistors.[2−5] Another application is metal oxide ALD on graphene or carbon nanotubes to deposit films for electrochemical energy storage.[6] Examples include metal oxide ALD for Li ion batteries[7−10] or supercapacitors.[11−13] A critical consideration for these uses of metal oxide ALD is preserving the electrical conductivity of the sp^2 carbon support after the deposition to maintain optimum device performance.[1]

The nucleation of metal oxide ALD films on sp^2 carbon surfaces has proven very challenging.[1] Because of the chemical inertness of sp^2 carbon surfaces, ALD surface chemistry is observed to nucleate only at defects or step edges. Al_2O_3 ALD utilizing trimethylaluminum (TMA) and water (H_2O) nucleates only on the defects of single and multiwalled carbon nanotubes.[14,15] Al_2O_3 and HfO_2 ALD forms nanoribbons along the step edges of graphene.[16] The nucleation difficulties on sp^2 carbon surfaces are not limited to metal oxide ALD. Pt ALD is also observed to form nanowires along the step edges of highly ordered pyrolytic graphite (HOPG).[17] To deposit on more than defects and step edges, the chemically inert sp^2 carbon surface must be functionalized to obtain conformal metal oxide ALD films.

Various techniques have been developed to functionalize sp^2 carbon surfaces for subsequent metal oxide ALD.[1,18,19] For example, TMA and ozone have been demonstrated to facilitate Al_2O_3 ALD on graphene without any preferential deposition at the step edges because of surface functionalization resulting from the reaction of ozone with graphene.[20] Fluorine functionalization using XeF_2 has also been shown to yield conformal Al_2O_3 ALD films.[21] Various noncovalent organic seeding layers have also proved effective at functionalizing graphene for ALD.[22] The organic seeding layers for ALD include perylene tetracarboxylic acid,[23] perylene-3,4,9,10-tetracarboxylic dianhydride,[24] and poly(4-vinylphenol).[25] Various H_2O pretreatments have also been reported recently that facilitate the growth of Al_2O_3 ALD on graphene.[26−28]

Noncovalent functionalization chemistries that facilitate the nucleation of metal oxide ALD on sp^2 carbon surfaces without disrupting the graphene lattice have enabled dielectric deposition while avoiding degraded electrical performance.[1] One convenient vapor phase, noncovalent functionalization

Received: March 11, 2015
Accepted: May 12, 2015
Published: May 12, 2015

DOI: 10.1021/acsami.5b02167
ACS Appl. Mater. Interfaces 2015, 7, 12030−12037

technique involves pretreatment of carbon nanotubes using nitrogen dioxide (NO_2) and TMA.[29] The NO_2/TMA chemistry starts with NO_2 adsorption on the sp^2 carbon surface.[29] This NO_2 adsorption is followed by TMA exposure to cross-link the adsorbed NO_2 molecules and provide an "Al_2O_3-like" surface that serves as an adhesion layer for subsequent ALD film growth.[29]

The NO_2/TMA functionalization technique was originally performed on single-walled carbon nanotubes at 25 °C for subsequent Al_2O_3 ALD.[29] Additional efforts extended this technique to large quantities of multiwalled carbon nanotubes at higher temperatures for Al_2O_3 ALD and W ALD.[14] This NO_2/TMA pretreatment has also been employed to deposit ultrathin Al_2O_3 ALD films on graphene.[30] In addition, the NO_2/TMA pretreatment has been used for metal oxide ALD on graphene and carbon nanotubes for electrochemical energy storage applications. Examples include the use of the NO_2/TMA pretreatment to enable TiO_2 ALD on graphene to fabricate anodes for Li ion batteries[7] and TiO_2 on graphene and carbon nanotubes to fabricate charge storage layers for supercapacitors.[12]

In this paper, we examined Al_2O_3 adhesion layers deposited after five cycles of the NO_2/TMA pretreatment at 150 °C on HOPG. Al_2O_3 ALD growth on these Al_2O_3 adhesion layers on HOPG was then measured as a function of the number of TMA/H_2O ALD cycles using spectroscopic ellipsometry and electrochemical analysis. We also analyzed films deposited using a varying number of NO_2/TMA cycles at 150 °C on HOPG and Al_2O_3 surfaces. Comparisons with Al_2O_3 films grown on HOPG without the NO_2/TMA pretreatment revealed the effect of the NO_2/TMA pretreatment on the thickness and quality of the Al_2O_3 films.

II. EXPERIMENTAL SECTION

A. Sample Preparation. Model sp^2 carbon surfaces were prepared by exfoliating HOPG (SPI supplies SPI-2 grade 20 × 20 × 1 mm). This exfoliation was performed using conductive copper tape (3M single sided Cu conductive tape, 1 in width). This exfoliation procedure is illustrated in Figure 1a. The resulting HOPG film on the copper tape is shown in Figure 1b. ALD was then performed on these approximately square HOPG samples. After ALD growth, a 5/8 in diameter disc was punched out of the Al_2O_3/HOPG film on the copper tape as illustrated in Figure 1c. The resulting circular discs shown in Figure 1d were used for electrochemical analysis.

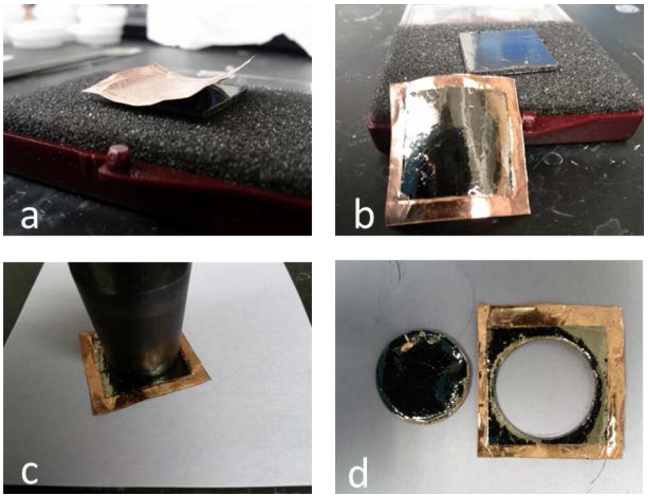

Figure 1. Photographs of the procedure used to prepare model sp^2 carbon surfaces: (a) exfoliation of HOPG onto copper tape, (b) HOPG film on copper tape following exfoliation, (c) punching out a disc of HOPG on copper tape, and (d) completed HOPG substrate on copper tape for electrochemical analysis.

Silicon witness wafers were also prepared using the following procedure to provide a comparison with the HOPG samples. Silicon samples with a native oxide and dimensions of ∼1 in. × 1 in. were cut from 6 in. silicon (Si) wafers (Silicon Valley Microelectronics). These samples were rinsed with acetone (Fisher, Certified ACS) and methanol (EMD Millipore HPLC grade) and dried using UHP nitrogen (Airgas). These Si witness wafers were placed in the reactor during the ALD on the HOPG samples.

B. ALD Growth. ALD was performed simultaneously on HOPG samples and Si witness wafers in a custom viscous-flow reactor.[31] The Al_2O_3 ALD was performed at 150 °C under a continuous argon gas flow (Airgas, Prepurified) at ∼1 Torr. The Al_2O_3 ALD films were grown using sequential exposures of (A) trimethylaluminum (TMA) (Aldrich 97%) and (B) water (H_2O) (B&J Brand HPLC grade). The peak exposure pressures for both precursors was adjusted to ∼200 mTorr above base pressure. The timing sequence for (A exposure, purge, B exposure, purge) during these TMA/H_2O cycles was (0.5 s, 45 s, 0.5 s, 45 s).

The NO_2/TMA pretreatment was performed using (C) NO_2 (Aldrich ≥99.5%) and (A) TMA. The NO_2/TMA pretreatment was also performed at 150 °C under continuous argon gas flow at ∼1 Torr. The peak exposure pressures for both precursors were adjusted to ∼200 mTorr above argon base pressure. The timing sequence for (C exposure, purge, A exposure, purge) during these NO_2/TMA cycles was (0.2 s, 45 s, 0.5 s, 45 s).

C. Sample Characterization. The thickness and density of the ALD coatings on the Si witness wafers were evaluated using X-ray reflectivity (XRR). XRR measurements were performed using a Bede D-1 Diffractometer. X-ray radiation with a wavelength of 1.54 Å corresponding to the Cu−Kα transition was used for these measurements. The film thicknesses and densities were modeled using the Bede REFS software.

The thicknesses of the ALD films on the HOPG samples were evaluated using spectroscopic ellipsometry (SE). SE measurements were performed using a M-2000 spectroscopic ellipsometer (J.A. Woollam Co., Inc.). Film properties were modeled using CompleteEASE v.4.55 (J.A. Woollam Co., Inc.). A Kramers−Kronig consistent B-spline model was used for the HOPG substrate.[32] A Cauchy model was used for the ALD films.[33] The ALD film thicknesses on the Si witness wafers were also determined by SE and compared with the XRR measurements.

D. Electrochemical Evaluation. The porosity of insulating films on conducting substrates can be evaluated by determining the charge-transfer resistance at the open-circuit potential.[34−36] Electrochemical impedance spectroscopy (EIS) and linear sweep voltammetry (LSV) were performed on the ALD-coated HOPG samples to determine charge-transfer resistances. These electrochemical measurements utilized a 2-channel SP-300 potentiostat with low current probes from BioLogic. A Faraday cage surrounded the electrochemical cell during measurements to reduce electrical noise for low measured currents. EIS measurements were performed from 3 MHz to 10 mHz with a sinusoidal amplitude of 5 mV using multisine measurements for low frequencies. The EIS data was fit using the EC-Lab software from BioLogic.

LSV was performed at a sweep rate of 1 mV/s in a 200 mV window surrounding the open-circuit potential. The slope of the current−voltage (I−V) curve at zero current was used to determine the charge transfer resistance. Electrochemical measurements were performed in custom electrochemical cells with an internal volume of ∼25 mL. A 0.10 M sodium sulfate aqueous electrolyte (pH = ∼6) was prepared using sodium sulfate powder (Alfa Aesar, 99.99% metals basis) and deionized water (>18.2 MΩ resistance). Prior to electrochemical measurements, the electrolyte was purged for >10 min using argon (Airgas, Prepurified) and a continuous argon purge was maintained during the experiments. Platinum counter electrodes and saturated

DOI: 10.1021/acsami.5b02167
ACS Appl. Mater. Interfaces 2015, 7, 12030−12037

Ag/AgCl reference electrodes (BASi) were used for these electrochemical measurements.

Dissolution experiments were performed in the electrochemical cell. Consequently, the electrochemical measurements could be conducted in situ without having to transfer the sample between the dissolution bath and the electrochemical cell. The dissolution and electrochemical measurements were performed at room temperature. The same 0.10 M sodium sulfate aqueous solution was used throughout the course of each dissolution experiment. In addition, the argon purge was also maintained during the dissolution experiment.

III. RESULTS AND DISCUSSION

A. Al_2O_3 Film Growth on HOPG and Silicon. Figure 2 shows the film thickness after 0−200 Al_2O_3 ALD cycles of TMA/H_2O with and without the NO_2/TMA pretreatment on the HOPG samples at 150 °C. The Al_2O_3 ALD growth rate on HOPG was determined to be 1.4 Å/cycle. This Al_2O_3 ALD growth rate agrees well with previously reported growth rates of ∼1.2 Å/cycle at 150 °C.[31,37,38] The NO_2/TMA pretreatment using five cycles of NO_2 and TMA also results in an estimated Al_2O_3 adhesion layer thickness of ∼8.2 Å on the HOPG samples as determined by the y-intercept in Figure 2.

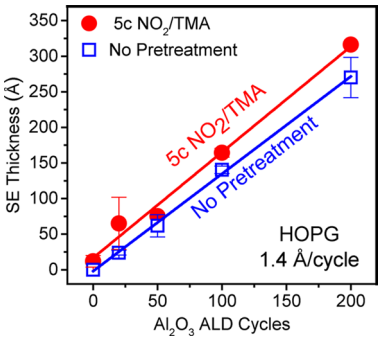

Figure 2. Spectroscopic ellipsometry measurements of Al_2O_3 film thickness on HOPG versus Al_2O_3 ALD cycles with and without five cycles of NO_2/TMA pretreatment at 150 °C.

In comparison, the thickness after 0−200 Al_2O_3 ALD cycles of TMA/H_2O with and without the NO_2/TMA pretreatment on Si witness wafers at 150 °C is shown in Figure 3. The Al_2O_3 ALD growth rate on Si was 1.3 Å/cycle. Figure 3 shows that no Al_2O_3 thickness was detected and no Al_2O_3 was deposited after the NO_2/TMA pretreatment using five cycles of NO_2 and TMA on the Si witness wafers. This behavior contrasts with the results in Figure 2. The NO_2/TMA pretreatment deposits an Al_2O_3 adhesion layer on the HOPG samples, but not on the Si witness wafers.

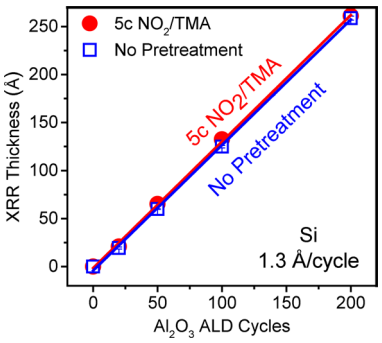

Figure 3. XRR measurements of the Al_2O_3 film thickness on Si versus Al_2O_3 ALD cycles with and without five cycles of NO_2/TMA pretreatment at 150 °C.

Figure 4 shows Al_2O_3 film growth versus NO_2/TMA cycles on both HOPG and an Al_2O_3 ALD film at 150 °C. Consistent with the results in Figure 2, Al_2O_3 film growth is observed on the HOPG surface. After five cycles of NO_2/TMA, the thickness of the Al_2O_3 film on the HOPG substrates is measured to be 5.7 ± 3.6 Å. This thickness is consistent with the ∼8.2 Å estimated thickness obtained from the y-intercept in Figure 2. After 10 cycles of NO_2/TMA, an Al_2O_3 film with a thickness of 14.4 ± 1.3 Å is deposited on the HOPG substrates.

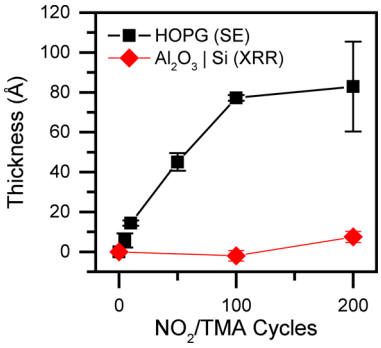

Figure 4. Al_2O_3 film thickness versus NO_2/TMA cycles at 150 °C on HOPG substrates and on silicon wafers coated with an Al_2O_3 ALD film with a thickness of ∼25 nm.

A previous investigation employed the NO_2/TMA pretreatment to deposit ultrathin Al_2O_3 ALD films on graphene.[30] This study measured an Al_2O_3 film thickness of 28 ± 3 Å using transmission electron microscopy (TEM) after 10 cycles of NO_2/TMA and five cycles of TMA/H_2O using static precursor dosing at 180 °C.[30] Assuming a growth rate of 1.2 Å/cycle for Al_2O_3 ALD using TMA/H_2O,[31,37,38] the Al_2O_3 film thickness of 28 ± 3 Å measured using TEM suggests that 10 NO_2/TMA cycles deposit an Al_2O_3 film thickness of ∼22 Å on graphene. This thickness is larger than the Al_2O_3 film thickness of 14.4 ± 1.3 Å on HOPG observed for 10 cycles of NO_2/TMA at 150 °C. The larger Al_2O_3 film thickness on graphene could be explained by the higher temperature of 180 °C and/or the static dosing used for the Al_2O_3 growth.

Figure 4 shows that the Al_2O_3 film growth continues for 100 NO_2/TMA cycles before reaching a limiting thickness of ∼80 Å. To verify this limiting thickness, the measurements after 200 NO_2/TMA cycles on HOPG samples were repeated on nine separate samples. These surprising results suggest that the growth of Al_2O_3 on graphite using NO_2/TMA cycles is dependent on the adsorption of NO_2 on the HOPG surface. Al_2O_3 growth using NO_2/TMA may terminate when NO_2 can no longer adsorb on the HOPG surface.

NO_2 is known to adsorb to carbon nanotube surfaces.[29,39,40] NO_2 is an electron acceptor and density functional theory (DFT) calculations have shown that charge transfers from the carbon nanotube to NO_2.[39] Other DFT calculations reveal that the adsorption of two neighboring NO_2 molecules on the carbon nanotube surface is more energetically favorable than the adsorption of isolated NO_2 molecules.[40,41] NO_2 is also an electron acceptor on graphene surfaces.[42] Results from graphene gas sensor experiments are consistent with electron transfer from graphene to NO_2 that produce hole carriers in graphene.[43]

DOI: 10.1021/acsami.5b02167
ACS Appl. Mater. Interfaces 2015, 7, 12030−12037

NO_2 has also been studied on graphite surfaces. The NO_2 adsorption energy was determined to be approximately −0.4 eV using temperature programmed desorption (TPD) studies.[44] NO_2 also adsorbs as a dimer, N_2O_4, on graphite.[44,45] Computational studies predict that the adsorption energy of NO_2 on pristine graphene is −0.5 eV. However, the adsorption energy of NO_2 at a defect site on graphene could be as much as −3 eV.[46] Although the adsorption energy of NO_2 on pristine graphite may be low, the residence time for NO_2 on graphite should be sufficiently long for NO_2 to react with TMA in the presence of defects and step edges on graphite.

Adsorbed NO_2 is expected to react with TMA according to the reaction

$$2Al(CH_3)_3 + 12NO_2 \rightarrow 6CO_2 + Al_2O_3 + 9H_2O + 6N_2 \quad (1)$$

This reaction has a very favorable Gibbs free energy of $\Delta G = -1687$ kcal/(mol Al_2O_3) at 150 °C.[47] This reaction may produce islands of Al_2O_3 deposited around defect sites on the HOPG substrate similar to the nucleation of Al_2O_3 ALD on carbon nanotubes.[14,29] The Al_2O_3 islands may then act as an electron donor to the graphene surface resulting from the negative fixed charge in Al_2O_3 ALD material.[48−50] The accumulation of negative charge in the graphene surrounding an Al_2O_3 island would further enhance adsorption of electron-accepting NO_2 during subsequent NO_2 exposures. In addition, the combustion reaction given in eq 1 produces H_2O. This H_2O product from the reaction of TMA with NO_2 adsorbed on HOPG or the reaction of NO_2 with Al-CH_3 species on Al_2O_3 may facilitate additional Al_2O_3 growth.

The limiting Al_2O_3 film thickness of ∼80 Å for NO_2/TMA growth on HOPG may be explained by the negligible Al_2O_3 growth using NO_2/TMA cycles on an Al_2O_3 surface as observed in Figure 4. The starting Al_2O_3 surface in Figure 4 was obtained by depositing 200 Al_2O_3 ALD cycles using TMA/H_2O on a Si wafer. The thickness of this Al_2O_3 ALD film was 259 ± 2 Å. For this Al_2O_3 ALD film, only negligible Al_2O_3 film growth was observed even after 200 NO_2/TMA cycles at 150 °C. The lack of Al_2O_3 growth on Al_2O_3 ALD films during NO_2/TMA cycles is attributed to weak adsorption of NO_2 on Al_2O_3. Weak NO_2 adsorption decreases the residence time of NO_2 on the Al_2O_3 surface and limits Al_2O_3 growth. This explanation is supported by DFT calculations that showed only a −0.5 eV adsorption energy for NO_2 on the (100) surface of γ-Al_2O_3.[51] This explanation is also supported by TPD studies that observed <0.1 monolayer of NO_2 on θ-Al_2O_3 surfaces above 160 K.[52]

The limiting thickness of ∼80 Å for Al_2O_3 growth using NO_2/TMA on HOPG is believed to be correlated with the deposition of a continuous Al_2O_3 film that prevents NO_2 adsorption. After this continuous Al_2O_3 film forms, NO_2 cannot adsorb on the HOPG surface. At this point, the Al_2O_3 film on HOPG is equivalent to the thick Al_2O_3 ALD film on silicon. No growth of Al_2O_3 is observed by NO_2/TMA cycles on the Al_2O_3 ALD film on silicon. The growth of Al_2O_3 on HOPG using NO_2/TMA illustrates surface-selective and self-terminating behavior that may be useful for future applications.

B. Electrochemical Measurements. Figure 5a shows measured EIS spectra and model fits for the HOPG samples with 0−200 Al_2O_3 ALD cycles without the NO_2/TMA pretreatment. In this Nyquist plot, the radius of the semicircle is indicative of the charge-transfer resistance for the electrode/electrolyte interface. A smaller radius indicates a lower charge-transfer resistance. The measured charge-transfer resistances are smaller than the uncoated HOPG substrate after 20 and 50 ALD cycles. In contrast, the charge-transfer resistances are larger than those of the uncoated HOPG substrate after 100 and 200 ALD cycles.

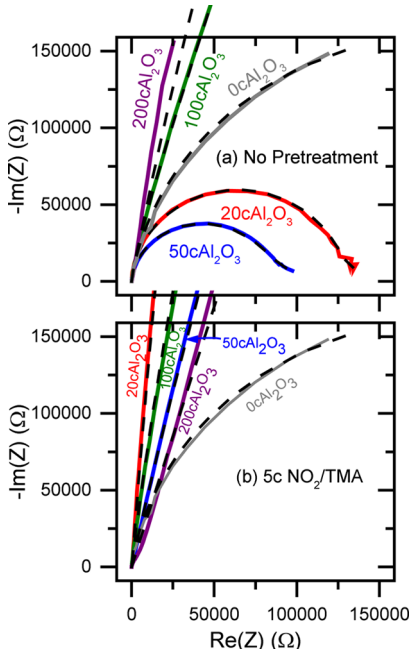

Figure 5. Nyquist plot of EIS results for (a) Al_2O_3 ALD on HOPG substrates with no pretreatment and (b) Al_2O_3 ALD on HOGP substrates after five cycles of NO_2/TMA pretreatment. The dashed lines show model fits to the EIS data.

Figure 5b displays measured EIS spectra and model fits for the HOPG samples with 0−200 Al_2O_3 ALD cycles with the NO_2/TMA pretreatment. With the Al_2O_3 adhesion layer, the charge-transfer resistances are all larger than the uncoated HOPG substrate after 20, 50, 100, and 200 Al_2O_3 ALD cycles. However, the EIS measurements may not have the accuracy to distinguish differences among these large charge-transfer resistances.

Figure 6 shows the model circuit used to fit the EIS data.[53] "R" indicates a resistor and "Q" indicates a constant phase element (CPE). This model circuit represents possible electrochemical processes occurring at the electrolyte interface of a conductor with an insulating coating containing through-film porosity.[34−36] In this circuit, R_1 represents the sum of ionic resistance in the bulk electrolyte and electrical resistance in the bulk metal substrate. Q_1 represents the capacitance of the insulating film. R_2 represents ionic resistance in the through-film pores of the insulating film. Q_3/R_3 represents a Faradaic process at the metal−electrolyte interface in the through-film pores of the insulating film. This model circuit allows

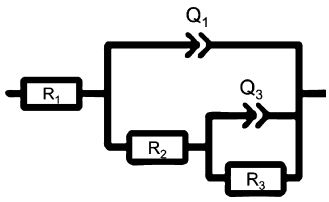

Figure 6. Model equivalent circuit used to fit the EIS measurements.

DOI: 10.1021/acsami.5b02167
ACS Appl. Mater. Interfaces 2015, 7, 12030−12037

comparison of the through-film porosity of different insulating coatings by fitting EIS data with this circuit.

The total charge-transfer resistances versus number of Al_2O_3 ALD cycles on HOPG from both the EIS and LSV measurements are shown in Figure 7. The modeled values

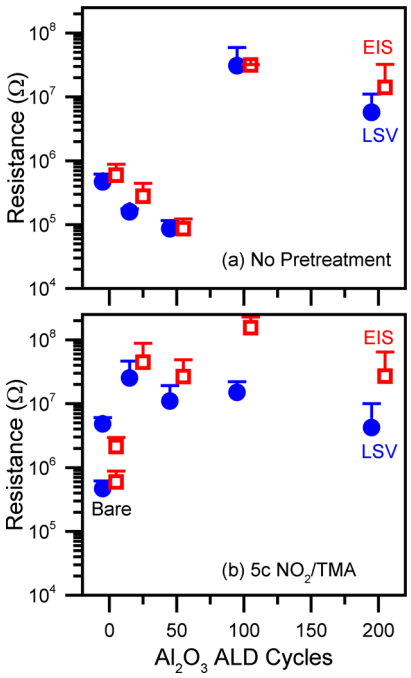

Figure 7. Charge-transfer resistance versus number of Al_2O_3 ALD cycles from EIS and LSV measurements for (a) Al_2O_3 ALD on HOPG substrates with no pretreatment and (b) Al_2O_3 ALD on HOGP substrates after five cycles of NO_2/TMA pretreatment.

from Figure 5a with no NO_2/TMA pretreatment are displayed in Figure 7a. The initial charge-transfer resistance is 0.6 MΩ by EIS. The charge-transfer resistance increases to 14 MΩ by EIS after 200 Al_2O_3 ALD cycles. The modeled values from Figure 5b after the NO_2/TMA pretreatment are given in Figure 7b. The initial charge-transfer resistance is 2 MΩ by EIS after the NO_2/TMA pretreatment. The charge-transfer resistance increases to 27 MΩ by EIS after 200 Al_2O_3 ALD cycles.

With no NO_2/TMA pretreatment, the Al_2O_3 ALD chemistry will nucleate at step edges and defect sites on the HOPG surface.[14,16] The Al_2O_3 deposition is expected to be in the form of islands as shown schematically in Figure 8a. After a sufficient number of ALD cycles, the islands will grow together and the Al_2O_3 deposition will form a continuous film as illustrated in Figure 8a. In contrast, Al_2O_3 islands are more rapidly formed at defect sites on the HOPG surface after five cycles of NO_2/TMA. The higher density of Al_2O_3 islands produces a more continuous Al_2O_3 nucleation layer on the HOPG surface. Subsequently, the TMA/H_2O ALD cycles yield a more conformal Al_2O_3 film as illustrated in Figure 8b.

The charge-transfer resistances after 20 and 50 ALD cycles on the HOPG substrate with no NO_2/TMA pretreatment are given in Figure 7a. These charge-transfer resistances are *smaller* than the initial charge-transfer resistance. This behavior was unexpected because Al_2O_3 is an insulating material.[54] The initial nucleation of Al_2O_3 at step edges and defect sites on HOPG and subsequent growth after 20 and 50 Al_2O_3 ALD cycles were anticipated to lead to an increase in charge-transfer resistance.

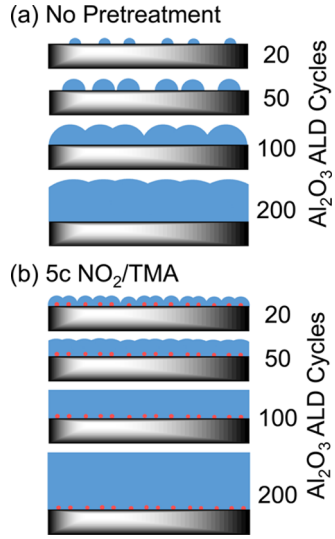

Figure 8. Schematic of film growth for (a) Al_2O_3 ALD on HOPG substrates with no pretreatment and (b) Al_2O_3 ALD on HOGP substrates after five cycles of NO_2/TMA pretreatment.

On the basis of previous studies,[1,14−16] these Al_2O_3 ALD films after 20 and 50 Al_2O_3 ALD cycles are not expected to be continuous on the HOPG substrate as illustrated in Figure 8a. Without complete coverage of the HOPG surface, Al_2O_3 ALD films should not be effective insulators because of the pinholes or extremely thin areas resulting from the nucleation difficulties. The expected poor conformality for these films would account for a relatively small increase in resistance for these films, but does not provide an explanation for the observed *decrease* in charge transfer resistance.

To interpret this decrease in charge transfer resistance, consider the determination of these values from LSV measurements. During LSV, the current is measured while the potential is scanned slowly at 1 mV/s in a 200 mV window surrounding the open-circuit potential. The charge transfer resistance is determined from the slope of the current−voltage curve as the current crosses zero. A greater change in current with changing potential yields a lower charge transfer resistance.

A lower charge transfer resistance could be attributed to a number of explanations. (1) Hydrophilic Al_2O_3 islands or extremely thin Al_2O_3 films may help break down ion solvation shells and enable ions to adsorb closer to the HOPG electrode surface. (2) Specific adsorption of cations may be facilitated by electron donation from Al_2O_3 islands to the graphite surface, enabling more cations to adsorb. (3) A redox process may be occurring in the Al_2O_3, such as proton incorporation into Al_2O_3 or dissolution of Al_2O_3. These explanations could lead to a lower measured charge transfer resistance.

In contrast, the charge-transfer resistances versus Al_2O_3 ALD cycles on the HOPG sample after five NO_2/TMA cycles show a qualitatively different behavior. The charge-transfer resistances all increase with Al_2O_3 ALD cycles after the NO_2/TMA pretreatment. This behavior is consistent with the continuous growth of a conformal Al_2O_3 film with Al_2O_3 ALD cycles as illustrated in Figure 8b. With the NO_2/TMA pretreatment, the electron conductivity is too low for the electron transport required for ion adsorption or redox processes.

C. Effective Film Porosities and Film Dissolution. The total charge-transfer resistances obtained from the EIS and LSV

DOI: 10.1021/acsami.5b02167
ACS Appl. Mater. Interfaces 2015, 7, 12030−12037

measurements were used to estimate the effective porosity of the Al_2O_3 films according to[34]

$$P \cong \frac{R_{bare}}{R_{coated}} \quad (2)$$

In this equation, P is the fractional effective porosity of the coating; R_{bare} is the total charge-transfer resistance of the bare substrate ($R_1 + R_2 + R_3$); and R_{coated} is the total charge-transfer resistance of the coated substrate. The effective porosities of Al_2O_3 films with no pretreatment and with a five cycle NO_2/TMA pretreatment are shown in Figures 9a and 9b, respectively.

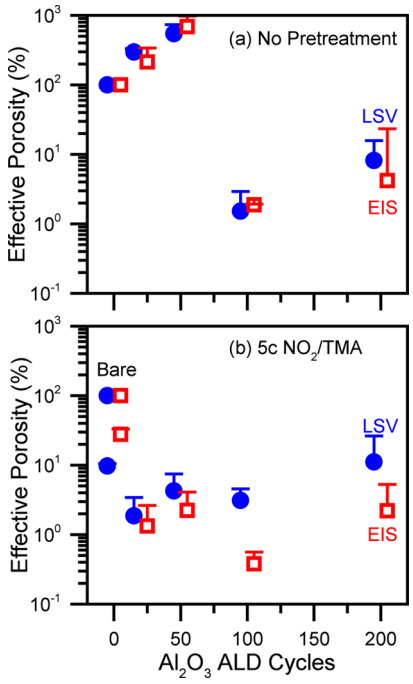

Figure 9. Effective porosity versus Al_2O_3 ALD cycles from EIS and LSV measurements for (a) Al_2O_3 ALD on HOPG substrates with no pretreatment and (b) Al_2O_3 ALD on HOGP substrates after five cycles of NO_2/TMA pretreatment.

The effective porosities in Figure 9a after 20 and 50 Al_2O_3 ALD cycles are >100%. These porosities larger than 100% result from charge transfer resistances that are lower than the initial HOPG substrate as described above. The porosities then decrease to <10% after 100 and 200 Al_2O_3 ALD cycles. In comparison, the effective porosity for all the Al_2O_3 film thicknesses in Figure 9b after five cycles of NO_2/TMA pretreatment is <10%. The EIS measurements reveal that the effective porosities after 100 and 200 Al_2O_3 ALD cycles are <1−2%. These results indicate that the NO_2/TMA pretreatment enables higher quality Al_2O_3 films on the HOPG surface than is obtained without NO_2/TMA pretreatment.

Additional experiments explored the dissolution of the Al_2O_3 films on the HOPG substrates. The dissolution was monitored by measuring the effective porosity of the Al_2O_3 film versus submersion time in water at room temperature. Figure 10 shows the effective porosity of the Al_2O_3 films versus time in 0.10 M aqueous sodium sulfate electrolyte. Figure 10a shows the measurements for an Al_2O_3 film grown on HOPG using 200 Al_2O_3 ALD cycles without the NO_2/TMA pretreatment. Figure 10b displays the measurements for an Al_2O_3 film grown

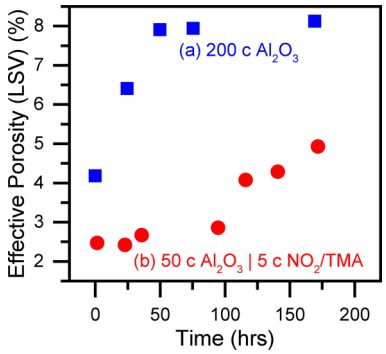

Figure 10. Effective porosity versus time in 0.10 M Na_2SO_4 aqueous electrolyte from LSV measurements on Al_2O_3 films on HOPG after (a) 200 Al_2O_3 ALD cycles with no pretreatment and (b) 50 Al_2O_3 ALD cycles with five cycles of NO_2/TMA pretreatment.

on HOPG using 50 Al_2O_3 ALD cycles after the five cycle NO_2/TMA pretreatment.

Figure 10a shows that the Al_2O_3 film grown using 200 Al_2O_3 ALD cycles with no NO_2/TMA pretreatment displays an increase in porosity almost immediately. This Al_2O_3 film had an initial thickness of ∼250 Å and an effective porosity of ∼4%. The porosity increased to ∼6.5% after 25 h and ∼8% after 50 h. The corrosion of Al_2O_3 ALD films in water at 25 and 90 °C has been observed previously.[55] The earlier observation of dissolution of Al_2O_3 ALD films in water was performed using optical microscopy and ellipsometry measurements.[55]

In contrast, Figure 10b shows that the stability is higher for the Al_2O_3 film grown using 50 Al_2O_3 ALD cycles after the five cycle NO_2/TMA pretreatment. This Al_2O_3 film had an initial thickness of ∼90 Å and an effective porosity of ∼2.5%. The porosity did not increase for ∼100 h. The effective porosity was only ∼5% after 175 h. These dissolution measurements indicate that the Al_2O_3 films grown on the HOGP substrate after the five cycle NO_2/TMA pretreatment have a higher stability in aqueous solution.

IV. CONCLUSIONS

The growth of Al_2O_3 ALD films on model sp^2-graphitic carbon substrates was examined after an NO_2/TMA pretreatment to deposit an Al_2O_3 adhesion layer. TMA and H_2O were used to grow Al_2O_3 ALD films on exfoliated HOPG at 150 °C with and without the pretreatment procedure consisting of five NO_2/TMA cycles. The Al_2O_3 films on the HOPG samples were evaluated using spectroscopic ellipsometry and electrochemical analysis to determine film thickness and film quality. These experiments revealed that five cycles of NO_2/TMA at 150 °C deposit an Al_2O_3 adhesion layer with a thickness of 5.7 ± 3.6 Å on HOPG.

An increased number of NO_2/TMA pretreatment cycles produced thicker Al_2O_3 films on HOPG until reaching a limiting thickness of ∼80 Å after 100 NO_2/TMA cycles. This Al_2O_3 growth was self-terminating with no additional Al_2O_3 film thickness observed after 200 NO_2/TMA cycles. The termination of Al_2O_3 growth is believed to be caused by the formation of a continuous Al_2O_3 film on the HOPG substrate. The Al_2O_3 film can grow if NO_2 can adsorb to the HOPG substrate. A continuous Al_2O_3 film on HOPG prevents NO_2 adsorption and terminates growth. This explanation was supported by negligible growth of Al_2O_3 on Al_2O_3 ALD films on silicon substrates using NO_2/TMA cycles.

DOI: 10.1021/acsami.5b02167
ACS Appl. Mater. Interfaces 2015, 7, 12030−12037

The EIS measurements showed that five cycles of the NO_2/TMA pretreatment produced high-quality insulating Al_2O_3 films with high charge-transfer resistances after as few as 20 Al_2O_3 ALD cycles using TMA/H_2O. In contrast, the EIS measurements revealed that 100 Al_2O_3 ALD cycles of TMA/H_2O were needed to produce an insulating film with high charge-transfer resistance without the NO_2/TMA pretreatment. In addition, Al_2O_3 films grown after the NO_2/TMA pretreatment at 150 °C also had much better resistance to dissolution in aqueous solutions.

AUTHOR INFORMATION

Corresponding Author

*E-mail: Steven.George@colorado.edu.

Notes

Any opinion, findings, and conclusions or recommendations expressed in this material are those of the authors(s) and do not necessarily reflect the views of the National Science Foundation.

The authors declare no competing financial interest.

ACKNOWLEDGMENTS

This research was funded by DARPA. M.J.Y. was supported by a National Science Foundation Graduate Research Fellowship under Grant No. DGE 1144083. C.B.M. acknowledges the National Science Foundation for support through grant CHE-1214131.

REFERENCES

(1) Marichy, C.; Pinna, N. Carbon-Nanostructures Coated/Decorated by Atomic Layer Deposition: Growth and Applications. *Coord. Chem. Rev.* **2013**, *257*, 3232−3253.

(2) Schwierz, F. Graphene Transistors. *Nat. Nanotechnol.* **2010**, *5*, 487−496.

(3) Williams, J. R.; Dicarlo, L.; Marcus, C. M. Quantum Hall Effect in a Gate-Controlled P−N Junction of Graphene. *Science* **2007**, *317*, 638−641.

(4) Kim, S.; Nah, J.; Jo, I.; Shahrjerdi, D.; Colombo, L.; Yao, Z.; Tutuc, E.; Banerjee, S. K. Realization of a High Mobility Dual-Gated Graphene Field-Effect Transistor with Al_2O_3 Dielectric. *Appl. Phys. Lett.* **2009**, *94*, 20−23.

(5) Javey, A.; Kim, H.; Brink, M.; Wang, Q.; Ural, A.; Guo, J.; McIntyre, P.; McEuen, P.; Lundstrom, M.; Dai, H. High-K Dielectrics for Advanced Carbon-Nanotube Transistors and Logic Gates. *Nat. Mater.* **2002**, *1*, 241−246.

(6) Hou, J.; Shao, Y.; Ellis, M. W.; Moore, R. B.; Yi, B. Graphene-Based Electrochemical Energy Conversion and Storage: Fuel Cells, Supercapacitors and Lithium Ion Batteries. *Phys. Chem. Chem. Phys.* **2011**, *13*, 15384−15402.

(7) Ban, C.; Xie, M.; Sun, X.; Travis, J. J.; Wang, G.; Sun, H.; Dillon, A. C.; Lian, J.; George, S. M. Atomic Layer Deposition of Amorphous TiO_2 on Graphene as an Anode for Li-Ion Batteries. *Nanotechnology* **2013**, *24*, 424002.

(8) Jung, Y. S.; Cavanagh, A. S.; Riley, L. A.; Kang, S.-H. H.; Dillon, A. C.; Groner, M. D.; George, S. M.; Lee, S.-H. H. Ultrathin Direct Atomic Layer Deposition on Composite Electrodes for Highly Durable and Safe Li-Ion Batteries. *Adv. Mater.* **2010**, *22*, 2172−2176.

(9) Li, X. F.; Meng, X. B.; Liu, J.; Geng, D. S.; Zhang, Y.; Banis, M. N.; Li, Y. L.; Yang, J. L.; Li, R. Y.; Sun, X. L.; Cai, M.; Verbrugge, M. W. Tin Oxide with Controlled Morphology and Crystallinity by Atomic Layer Deposition onto Graphene Nanosheets for Enhanced Lithium Storage. *Adv. Funct. Mater.* **2012**, *22*, 1647−1654.

(10) Meng, X.; Yang, X.-Q.; Sun, X. Emerging Applications of Atomic Layer Deposition for Lithium-Ion Battery Studies. *Adv. Mater.* **2012**, *24*, 3589−3615.

(11) Boukhalfa, S.; Evanoff, K.; Yushin, G. Atomic Layer Deposition of Vanadium Oxide on Carbon Nanotubes for High-Power Supercapacitor Electrodes. *Energy Environ. Sci.* **2012**, *5*, 6872−6879.

(12) Sun, X.; Xie, M.; Travis, J. J.; Wang, G.; Sun, H.; Lian, J.; George, S. M. Pseudocapacitance of Amorphous TiO_2 Thin Films Anchored to Graphene and Carbon Nanotubes Using Atomic Layer Deposition. *J. Phys. Chem. C* **2013**, *117*, 22497−22508.

(13) Sun, X.; Xie, M.; Wang, G.; Sun, H.; Cavanagh, A. S.; Travis, J. J.; George, S. M.; Lian, J. Atomic Layer Deposition of TiO_2 on Graphene for Supercapacitors. *J. Electrochem. Soc.* **2012**, *159*, A364−A369.

(14) Cavanagh, A. S.; Wilson, C. A.; Weimer, A. W.; George, S. M. Atomic Layer Deposition on Gram Quantities of Multi-Walled Carbon Nanotubes. *Nanotechnology* **2009**, *20*, 255602.

(15) Farmer, D. B.; Gordon, R. G. ALD of High-K Dielectrics on Suspended Functionalized SWNTs. *Electrochem. Solid-State Lett.* **2005**, *8*, G89−G91.

(16) Xuan, Y.; Wu, Y. Q.; Shen, T.; Qi, M.; Capano, M. a.; Cooper, J. A.; Ye, P. D. Atomic-Layer-Deposited Nanostructures for Graphene-Based Nanoelectronics. *Appl. Phys. Lett.* **2008**, *92*, 90−93.

(17) Lee, H. B. R.; Baeck, S. H.; Jaramillo, T. F.; Bent, S. F. Growth of Pt Nanowires by Atomic Layer Deposition on Highly Ordered Pyrolytic Graphite. *Nano Lett.* **2013**, *13*, 457−463.

(18) Huang, X.; Yin, Z.; Wu, S.; Qi, X.; He, Q.; Zhang, Q.; Yan, Q.; Boey, F.; Zhang, H. Graphene-Based Materials: Synthesis, Characterization, Properties, and Applications. *Small* **2011**, *7*, 1876−1902.

(19) Tasis, D.; Tagmatarchis, N.; Bianco, A.; Prato, M. Chemistry of Carbon Nanotubes. *Chem. Rev.* **2006**, *106*, 1105−1136.

(20) Kim, J.; Lee, B.; Park, S. Y.; Kim, H. C.; Cho, K.; Vogel, E. M.; Kim, M. J.; Wallace, R. M. Conformal Al_2O_3 Dielectric Layer Deposited by Atomic Layer Deposition for Graphene-Based Nanoelectronics. *Appl. Phys. Lett.* **2008**, *92*, 1−4.

(21) Wheeler, V.; Garces, N.; Nyakiti, L.; Myers-Ward, R.; Jernigan, G.; Culbertson, J.; Eddy, C. J.; Gaskill, D. K.; Kurt Gaskill, D. Fluorine Functionalization of Epitaxial Graphene for Uniform Deposition of Thin High-K Dielectrics. *Carbon* **2012**, *50*, 2307−2314.

(22) Mann, J. A.; Dichtel, W. R. Noncovalent Functionalization of Graphene by Molecular and Polymeric Adsorbates. *J. Phys. Chem. Lett.* **2013**, *4*, 2649−2657.

(23) Wang, X.; Tabakman, S. M.; Dai, H. Atomic Layer Deposition of Metal Oxides on Pristine and Functionalized Graphene. *J. Am. Chem. Soc.* **2008**, *130*, 8152−8153.

(24) Alaboson, J. M. P.; Wang, Q. H.; Emery, J. D.; Lipson, A. L.; Bedzyk, M. J.; Elam, J. W.; Pellin, M. J.; Hersam, M. C. Seeding Atomic Layer Deposition of High-K Dielectrics on Epitaxial Graphene with Organic Self-Assembled Monolayers. *ACS Nano* **2011**, *5*, 5223−5232.

(25) Cheol Shin, W.; Yong Kim, T.; Sul, O.; Jin Cho, B. Seeding Atomic Layer Deposition of High-K Dielectric on Graphene with Ultrathin Poly(4-Vinylphenol) Layer for Enhanced Device Performance and Reliability. *Appl. Phys. Lett.* **2012**, *101*, 1−5.

(26) Cao, Y. Q.; Cao, Z. Y.; Li, X.; Wu, D.; Li, A. D. A Facile Way to Deposit Conformal Al_2O_3 Thin Film on Pristine Graphene by Atomic Layer Deposition. *Appl. Surf. Sci.* **2014**, *291*, 78−82.

(27) Zhang, Y.; Qiu, Z.; Cheng, X.; Xie, H.; Wang, H.; Xie, X.; Yu, Y.; Liu, R. Direct Growth of High-Quality Al_2O_3 Dielectric on Graphene Layers by Low-Temperature H_2O-Based ALD. *J. Phys. D. Appl. Phys.* **2014**, *47*, No. 055106.

(28) Zheng, L.; Cheng, X.; Cao, D.; Wang, G.; Wang, Z.; Xu, D.; Xia, C.; Shen, L.; Yu, Y.; Shen, D. Improvement of Al_2O_3 Films on Graphene Grown by Atomic Layer Deposition with Pre-H_2O Treatment. *ACS Appl. Mater. Interfaces* **2014**, *6*, 7014−7019.

(29) Farmer, D. B.; Gordon, R. G. Atomic Layer Deposition on Suspended Single-Walled Carbon Nanotubes via Gas-Phase Noncovalent Functionalization. *Nano Lett.* **2006**, *6*, 699−703.

(30) Wang, L.; Travis, J. J.; Cavanagh, A. S.; Liu, X.; Koenig, S. P.; Huang, P. Y.; George, S. M.; Bunch, J. S. Ultrathin Oxide Films by Atomic Layer Deposition on Graphene. *Nano Lett.* **2012**, *12*, 3706−3710.

DOI: 10.1021/acsami.5b02167
ACS Appl. Mater. Interfaces 2015, 7, 12030−12037

(31) Elam, J. W.; Groner, M. D.; George, S. M. Viscous Flow Reactor with Quartz Crystal Microbalance for Thin Film Growth by Atomic Layer Deposition. *Rev. Sci. Instrum.* **2002**, *73*, 2981−2987.
(32) Johs, B.; Hale, J. S. Dielectric Function Representation by B-Splines. *Phys. Status Solidi* **2008**, *205*, 715−719.
(33) Born, M.; Wolf, E. *Principles of Optics*, 6th ed.; Permagon Press: Cambridge, United Kingdom, 1980.
(34) Tato, W.; Landolt, D. Electrochemical Determination of the Porosity of Single and Duplex PVD Coatings of Titanium and Titanium Nitride on Brass. *J. Electrochem. Soc.* **1998**, *145*, 4173−4181.
(35) Ahn, S. H.; Choi, Y. S.; Kim, J. G.; Han, J. G. A Study on Corrosion Resistance Characteristics of PVD Cr−N Coated Steels by Electrochemical Method. *Surf. Coat. Technol.* **2002**, *150*, 319−326.
(36) Ahn, S. H.; Lee, J. H.; Kim, H. G.; Kim, J. G. A Study on the Quantitative Determination of Through-Coating Porosity in PVD-Grown Coatings. *Appl. Surf. Sci.* **2004**, *233*, 105−114.
(37) Groner, M. D.; Fabreguette, F. H.; Elam, J. W.; George, S. M. Low-Temperature Al_2O_3 Atomic Layer Deposition. *Chem. Mater.* **2004**, *16*, 639−645.
(38) Ott, A. W.; Klaus, J. W.; Johnson, J. M.; George, S. M.; Mccarley, K. C.; Way, J. D. Modification of Porous Alumina Membranes Using Al_2O_3 Atomic Layer Controlled Deposition. *Chem. Mater.* **1997**, *4756*, 707−714.
(39) Kong, J.; Franklin, N. R.; Zhou, C.; Chapline, M. G.; Peng, S.; Cho, K.; Dai, H. Nanotube Molecular Wires as Chemical Sensors. *Science* **2000**, *287*, 622−625.
(40) Seo, K.; Park, K. A.; Kim, C.; Han, S.; Kim, B.; Lee, Y. H. Chirality- and Diameter-Dependent Reactivity of NO_2 on Carbon Nanotube Walls. *J. Am. Chem. Soc.* **2005**, *127*, 15724−15729.
(41) Yim, W.-L.; Gong, X. G.; Liu, Z.-F. Chemisorption of NO_2 on Carbon Nanotubes. *J. Phys. Chem. B* **2003**, *107*, 9363−9369.
(42) Wehling, T. O.; Novoselov, K. S.; Morozov, S. V.; Vdovin, E. E.; Katsnelson, M. I.; Geim, A. K.; Lichtenstein, A. I. Molecular Doping of Graphene. *Nano Lett.* **2008**, *8*, 173−177.
(43) Pearce, R.; Iakimov, T.; Andersson, M.; Hultman, L.; Spetz, A. L.; Yakimova, R. Epitaxially Grown Graphene Based Gas Sensors for Ultra Sensitive NO_2 Detection. *Sens. Actuators, B* **2011**, *155*, 451−455.
(44) Sjövall, P.; So, S. K.; Kasemo, B.; Franchy, R.; Ho, W. NO_2 Adsorption on Graphite at 90 K. *Chem. Phys. Lett.* **1990**, *17*, 125−130.
(45) Moreh, R.; Finkelstein, Y.; Shechter, H. NO_2 Adsorption on Grafoil between 297 and 12 K. *Phys. Rev. B* **1996**, *53*, 16006−16012.
(46) Zhang, Y.-H.; Chen, Y.-B.; Zhou, K.-G.; Liu, C.-H.; Zeng, J.; Zhang, H.-L.; Peng, Y. Improving Gas Sensing Properties of Graphene by Introducing Dopants and Defects: A First-Principles Study. *Nanotechnology* **2009**, *20*, 185504.
(47) *HSC Chemistry*, 5.11 ed.; Outokumpu Research Oy: Pori, Finland.
(48) Agostinelli, G.; Delabie, A.; Vitanov, P.; Alexieva, Z.; Dekkers, H. F. W.; De Wolf, S.; Beaucarne, G. Very Low Surface Recombination Velocities on P-Type Silicon Wafers Passivated with a Dielectric with Fixed Negative Charge. *Sol. Energy Mater. Sol. Cells* **2006**, *90*, 3438−3443.
(49) Hoex, B.; Gielis, J. J. H.; Van De Sanden, M. C. M.; Kessels, W. M. M. On the c-Si Surface Passivation Mechanism by the Negative-Charge-Dielectric Al_2O_3. *J. Appl. Phys.* **2008**, *104*, 1−7.
(50) Shin, B.; Weber, J. R.; Long, R. D.; Hurley, P. K.; Van De Walle, C. G.; McIntyre, P. C. Origin and Passivation of Fixed Charge in Atomic Layer Deposited Aluminum Oxide Gate Insulators on Chemically Treated InGaAs Substrates. *Appl. Phys. Lett.* **2010**, *96*, 3−5.
(51) Liu, Z.; Li, J.; Woo, S. I.; Hu, H. Density Functional Theory Studies of NO and NO_2 Adsorption on Al_2O_3 Supported SnO_2 Cluster. *Catal. Lett.* **2013**, *143*, 912−918.
(52) Ozensoy, E.; Peden, C. H. F.; Szanyi, J. NO_2 Adsorption on Ultrathin Θ-Al_2O_3 Films: Formation of Nitrite and Nitrate Species. *J. Phys. Chem. B* **2005**, *109*, 15977−15984.
(53) Orazem, M. E.; Tribollet, B. *Electrochemical Impedance Spectroscopy*; John Wiley & Sons: Hoboken, NJ, 2008.
(54) Groner, M. D.; Elam, J. W.; Fabreguette, F. H.; George, S. M. Electrical Characterization of Thin Al_2O_3 Films Grown by Atomic Layer Deposition on Silicon and Various Metal Substrates. *Thin Solid Films* **2002**, *413*, 186−197.
(55) Abdulagatov, A. I.; Yan, Y.; Cooper, J. R.; Zhang, Y.; Gibbs, Z. M.; Cavanagh, A. S.; Yang, R. G.; Lee, Y. C.; George, S. M. Al_2O_3 and TiO_2 Atomic Layer Deposition on Copper for Water Corrosion Resistance. *ACS Appl. Mater. Interfaces* **2011**, *3*, 4593−4601.

DOI: 10.1021/acsami.5b02167
ACS Appl. Mater. Interfaces 2015, 7, 12030−12037